Int. J. Electrochem. Sci., 13 **(2018)** 2731 – 2744, doi: 10.20964/2018.03.53

International Journal of
ELECTROCHEMICAL
SCIENCE
www.electrochemsci.org

Effects of Reaction Conditions on the Morphology and Property of Sb Doped SnO_2 Nanorods Anode

Li Xu [1,2,*], *Huiying Duan* [1,2], *Ye Wang* [1,2], *Yuefei Lian* [1,2]

[1] School of Chemical Engineering and Technology, Tianjin University, Tianjin 300072, P. R. China
[2] Tianjin Key Laboratory of Membrane Science and Desalination Technology, Tianjin 300072, P. R. China
[*]E-mail: xuli620@163.com

Received: 19 November 2017 / *Accepted:* 12 January 2018 / *Published:* 5 February 2018

Sb-doped SnO_2 nanorods anodes were synthesized by a hydrothermal method with Ti sheets as substrates (Ti/SnO_2-Sb-NRs anodes). In this paper, we focus on the effects various preparing conditions, such as the acidity and basicity of the solution, precursor solvent, concentration, reaction temperature, growth time and annealing temperature, on the formation and electrochemical properties of SnO_2-Sb-NRs anodes. The surface morphology of SnO_2-Sb-NRs is investigated by scanning electron microscopy (SEM), and chronoamperometry (CA) is measured as an indirect assessment of the electrochemical performance of the anodes. It is shown that SnO_2-Sb-NRs can be synthesized in both strong acid solution and strong alkaline solution, and the microstructure of Sb-doped SnO_2 can be controlled to some extent by varying the reaction conditions. The Ti/SnO_2-Sb-NRs anode shows the best morphology and properties when the precursor concentration is 0.010 mol·L^{-1}, using ethanol-water (1:1, v/v) as the solvent, at 200 °C for 24 h, and annealing at 550 °C for 2 h. An electrochemical degradation experiment of Acid Red 73 (AR 73) verifies its good electro-catalytic performance. Moreover, the growth mechanism of the SnO_2-Sb-NRs is also discussed.

Keywords: Sb-doped SnO_2; Nanorods; Hydrothermal; Electrochemical oxidation; Optimal conditions.

1. INTRODUCTION

Over the past few decades, materials that have at least one dimension between 1 to 100 nm have attracted steadily growing interest. Researchers have found that both the chemical and physical properties could be improved in nanomaterials compared with bulk materials corresponding to the reduction in size and dimensionality [1]. Because of the abundance, special shape and superior

chemical and physical properties of one-dimensional (1D) inorganic semiconductor metal oxides, they are the focus of intensive research for potential applications [2,3].

Tin oxide (SnO_2) as an important n-type metal-oxide semiconductor with a band gap of 3.6 eV has been widely applied to lithium-ion batteries [4], gas sensors [5], photoelectrochemical cells [6] and electro-catalytic oxidation processes [7]. Since the 1D SnO_2 belt-like nanostructure was successfully synthesized in 2001 [8], tremendous efforts have been made to synthesize and characterize 1D SnO_2 nanostructures in the form of wires [4,9], lines [10,11], rods [12,13], and so forth [14,15]. Moreover, experimental studies have indicated that dopants such as Sb [16], Fe [17], or F [18] in SnO_2 can improve its electrical conductivity and other properties.

In general, the methods used to synthesize 1D-nanostructured SnO_2 include chemical vapor deposition (CVD) [19], thermal evaporation (TE) [20], templates [21], the anodic oxidation process [22], and the hydrothermal process [23]. Among them, hydrothermal synthesis is a method of preparing materials by simulating the mineralization mechanism in nature. It has wide application potential because of its convenient operation, mild conditions and economic viability for the large-scale preparation of SnO_2 nanostructures compared to other methods [24]. In previous studies by our research group, a novel SnO_2-Sb nanorods anode on a Ti sheet substrate (Ti/SnO_2-Sb-NRs anode) possessing excellent electrocatalytic performance was prepared using the hydrothermal process [25]. Generally, the morphological and catalytic properties of a material are closely related to the reaction conditions of the hydrothermal process and subsequent heat treatment [26]. However, the effects of the hydrothermal synthesis conditions on the performance of SnO_2-Sb nanorods anodes in wastewater treatment have not been further investigated.

To efficiently fabricate Sb-doped SnO_2 nanorods films with high performance by the hydrothermal method, the effects of reaction conditions, such as the precursor acidity or basicity, precursor solvent, precursor concentration, growth time, reaction temperature and annealing temperature are systematically investigated in this paper. The growth mechanism of SnO_2-Sb nanorods is also discussed.

2. EXPERIMENTAL

The fabrication a of Ti/SnO_2-Sb-NRs anode is performed according to our previous work [25]. After the pretreatment of a Ti sheet and the preparation of a Sn-Sb buffer layer by pulse electrodeposition, SnO_2-Sb-NRs are produced through a hydrothermal method. In a typical experiment, the precursor solution is created by dissolving $SnCl_4 \cdot 5H_2O$ (0.010 $mol \cdot L^{-1}$), $SbCl_3$ (1.429 $mmol \cdot L^{-1}$), $NaC_4H_5O_6 \cdot H_2O$ (4.286 $mmol \cdot L^{-1}$), NaOH (0.176 $mol \cdot L^{-1}$) and NaCl (1 $mol \cdot L^{-1}$) in a water-ethanol mixture (1:1, v/v) under magnetic stirring. Then, 35 mL of precursor solution and an electrode with a SnO_2-Sb buffer layer are transferred into a 50 mL Teflon-lined stainless-steel autoclave. The hydrothermal reaction is carried out at 200 °C for 24 h; after the reaction finished, the autoclave was cooled to room temperature naturally. At last, the electrode was rinsed repeatedly and annealed at 550 °C for 2 h.

To study the effect of the acidity or alkalinity of the solution, solvent and concentration on the preparation of SnO_2-Sb-NRs, hydrochloric acid or sodium hydroxide is added in the precursor solution, with pure deionized water and ethanol-water (1:1, v/v) chosen to be the solvent, and a molar ratio of $SnCl_4 \cdot 5H_2O$:$SbCl_3$:NaOH:$NaC_4H_5O_6 \cdot H_2O$:NaCl fixed at 1:0.143:17.6:0.429:100, the concentration of Sn^{4+} is varied from 0.0025 $mol \cdot L^{-1}$ to 0.015 $mol \cdot L^{-1}$. To investigate the effects of the hydrothermal reaction conditions, the reaction temperature is varied from 150 °C to 210 °C, and the reaction time is varied from 12 to 30 hours. The annealing temperature ranges from 500 °C to 600 °C to explore the effect on the electrocatalytic performance of SnO_2-Sb-NRs.

The morphologies of the Ti/SnO_2-Sb-NRs electrodes are examined by field emission scanning electron microscopy (SEM, S-4800, Hitachi, Japan). The electrochemical experiments for electrodes are carried out with an electrochemical workstation (PARSTAT 2273, PARC, USA) using a three-electrode cell system, with a Pt foil (40 mm×40 mm) as the counter electrode and Ag/AgCl/0.1 M KCl as the reference electrode. Chronoamperometry (CA) measurement is performed to test the electrocatalytic responses on each electrode at constant potential (1.0 and 2.5 V). The electrodes were first activated by cyclic voltammetry (CV) in a 0.5 M H_2SO_4 solution at 50 $mV \cdot s^{-1}$.

The electrochemical degradation test is performed in a glass vessel under a constant current density of 50 $mA \cdot cm^{-2}$ with magnetic stirring in a temperature-controlled bath (25 °C). The simulated wastewater consists of 1 $g \cdot L^{-1}$ Acid Red 73 (AR 73) solution (110 mL) whose supporting electrolyte is Na_2SO_4 (0.1 $mol \cdot L^{-1}$). The as-prepared Ti/SnO_2-Sb-NRs electrode is used as the anode, and a Ti sheet is used as the cathode with the same dimensions as the anode, and the gap between the two electrodes is 2 cm.

3. RESULTS AND DISCUSSION

3.1 Precursor solution

3.1.1 Effect of precursor acidity and basicity

Figure 1 shows two electrodes prepared with hydrochloric acid and sodium hydroxide. The results show that SnO_2-Sb-NRs can be synthesized in both a strong acid solution and a strong alkaline solution, and there are no significant differences between the morphologies of the two electrodes. However, concentrated hydrochloric acid erupts from the autoclave due to the high pressure generated from the high-temperature reaction and the hydrogen chloride gas escaping from the solution, which is dangerous to the operator and the environment. Like hydrochloric acid, urea and ammonia also release gases during hydrothermal reactions. By comparison, using sodium hydroxide to adjust the acidity or basicity of the precursor solution is safer. Therefore, in the following research, a strong alkaline precursor solution is prepared with sodium hydroxide.

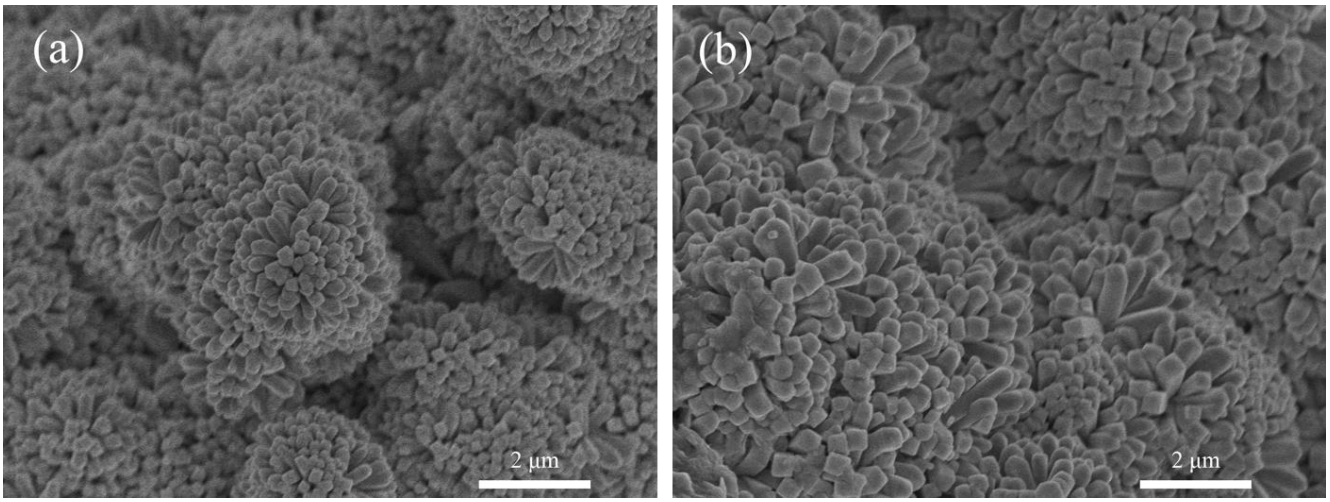

Figure 1. SEM images of electrodes prepared with acidic and alkaline solution (a) hydrochloric acid solution; (b) sodium hydroxide solution

3.1.2 Effect of solvent

In this experiment, pure deionized water and an ethanol-water mixture are chosen to be solvents. The reagents are difficult to dissolve when the proportion of ethanol is too high. To avoid this situation, the volume ratio of ethanol and deionized water is set as 1:1.

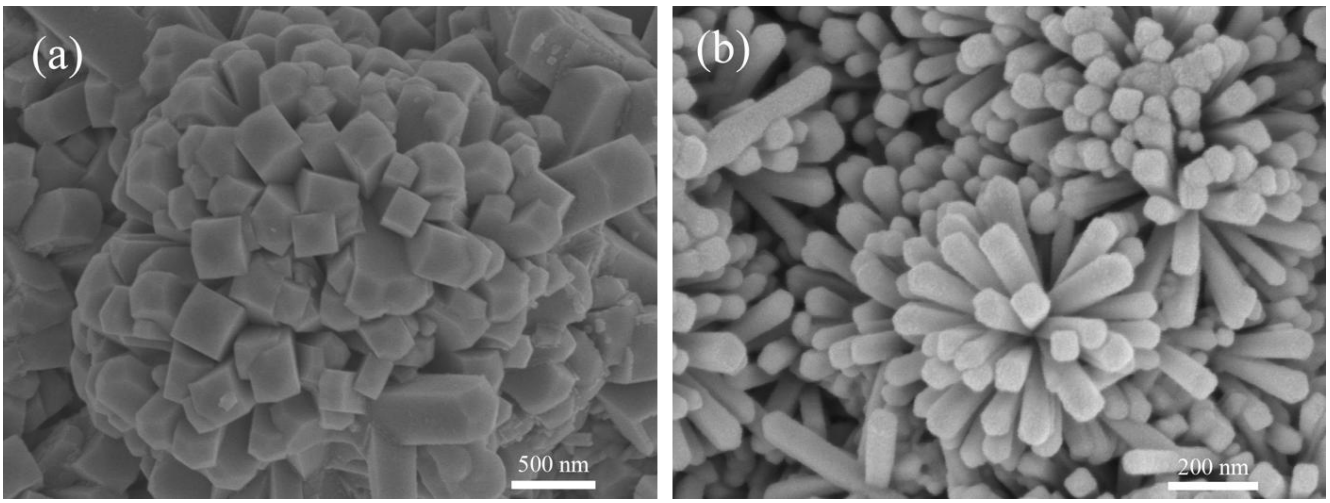

Figure 2. SEM images of electrodes prepared with solutions with various solvents (a) pure deionized water; (b) ethanol-water mixture (1:1, v/v)

It can be seen from Figure 2(a) and (b) that square column structures are distributed on the surface of both electrodes. The average width of the square columns on the surface of the electrode made with the ethanol-water mixture as a precursor solvent (ethanol-water group electrode) is approximately 70 nm. The distribution of these columns is relatively uniform, and there is no significant difference in the length among all columns. When using pure deionized water as the

solvent, the columns with poor dispersion easily agglomerate on the surface of the electrode (pure water group electrode). These square columns are arranged in a compact manner, causing serious constraints on the interior columns. While some columns distributed around can fully grow to achieve an average width approximately 350 nm, their length are longer. This may be due to ethanol playing a significant role in the crystal growth process of SnO_2-Sb. The water molecules prefer to bind with the ethanol molecules when water is mixed with ethanol. Thus, the dielectric constant of the solvent decreases, which increases the electrostatic interaction among the charged segments. Moreover, the H-bond network becomes less dense and forms disconnected clusters in the mixed solvent, leading to a loose structure [27].

3.1.3 Effect of concentrations

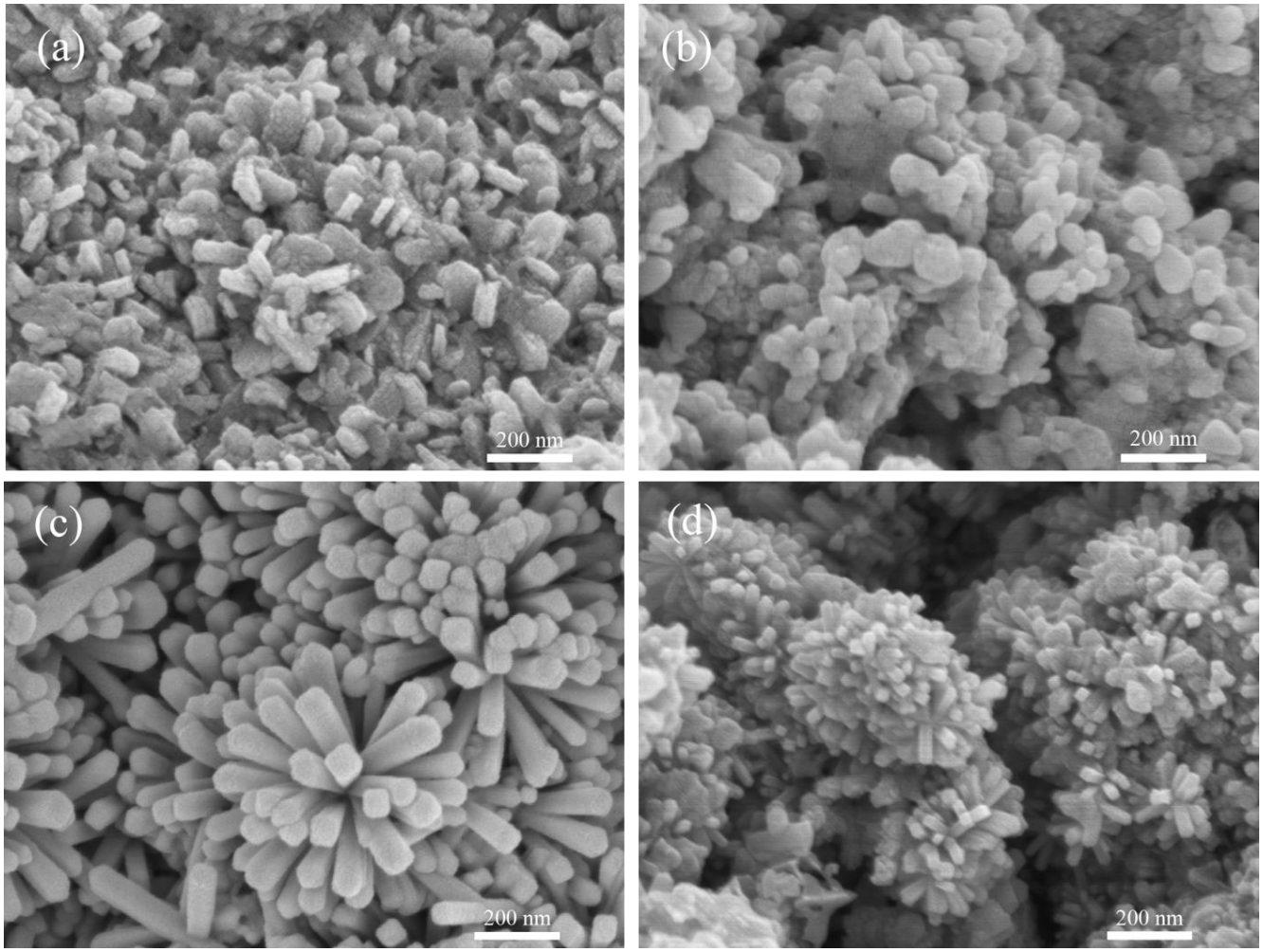

Figure 3. SEM images of the electrodes synthesized with different Sn^{4+} concentrations(a) 0.0025 $mol \cdot L^{-1}$; (b) 0.005 $mol \cdot L^{-1}$; (c) 0.010 $mol \cdot L^{-1}$; (d) 0.015 $mol \cdot L^{-1}$

The effects of different precursor concentrations on the growth of SnO_2-Sb nanostructures are shown in Figure 3. The morphology changes as the precursor concentration increases. As shown in

Figure 3(a) and (b), when the $SnCl_4$ concentration is 0.0025 mol·L^{-1} and 0.005 mol·L^{-1}, quasi-block and irregular spherical structures are distributed on the surfaces of the electrodes, respectively. As the concentration of $SnCl_4$ is further increased to 0.010 mol·L^{-1}, uniform nanorods are prepared (Figure 3(c)). When the precursor concentration increases to 0.015 mol·L^{-1}, square columns with an average width of approximately 30 nm cover the surface of electrode, but not all the columns can fully grow (Figure 3(d)).

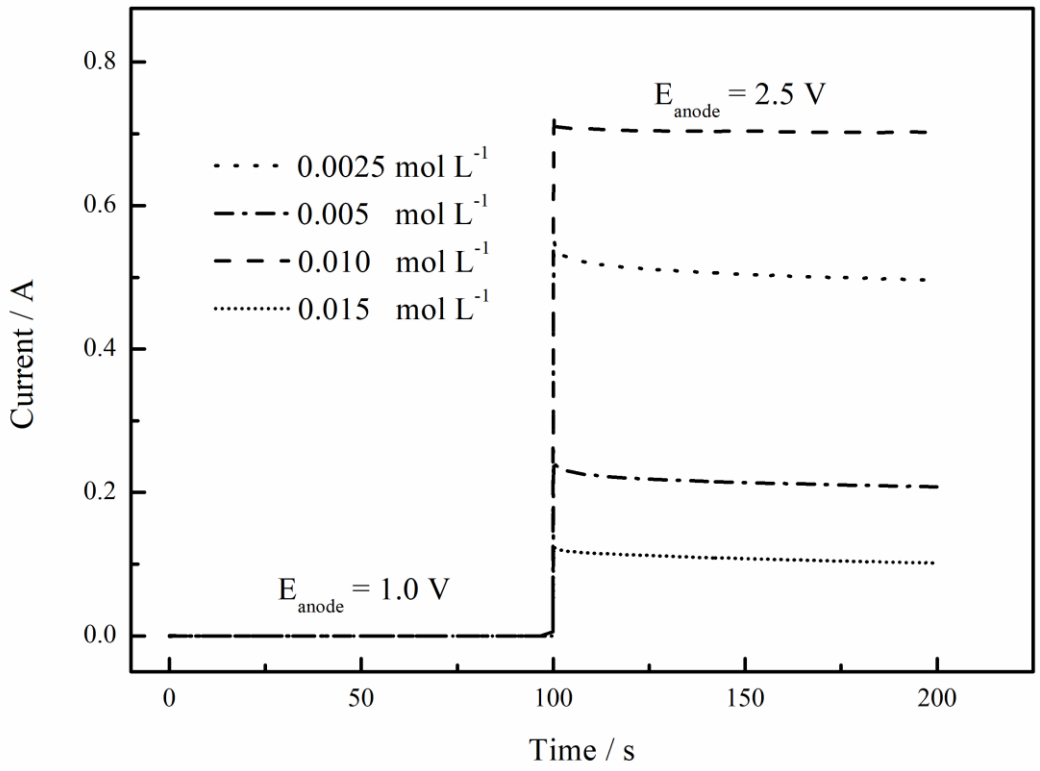

Figure 4. Chronoamperometric responses in a 0.5 M H_2SO_4 solution for electrodes synthesized with different Sn^{4+} concentrations

The chronoamperometry responses, *I*, of the different electrodes prepared with various precursor concentrations can be seen in Figure 4, and $I_{0.015\ mol/L}$ = 0.10 A < $I_{0.005\ mol/L}$ = 0.21 A < $I_{0.0025\ mol/L}$ = 0.50 A < $I_{0.010\ mol/L}$ = 0.70 A. There is reason to believe that the precursor concentration has an obvious influence on the morphology and properties of the synthesized products. This might be attributed to the nucleation and growth of the crystals during the hydrothermal reaction. A relatively high Sn^{4+} concentration can accelerate the nucleation process and lead to a higher nuclei concentration with a number of small nuclei [28,29], but the fast crystal growth speed in the initial stage leads to rapid consumption of the growth units, which restricts the crystal growth later in the process, causing severe lattice disorder [12]. Under these circumstances, the direct and effective transfer of electric charges is obstructed. Although no nanorod-like morphologies appear when using a precursor

concentration of 0.0025 mol·L^{-1} or 0.005 mol·L^{-1}, the lower growth speed causes a relatively complete crystal development, and thus, their properties are better than those of the electrode prepared in a concentration of 0.015 mol·L^{-1}. In comparison, when the concentration of Sn^{4+} is 0.010 mol·L^{-1}, the crystal growth rate is suitable and forms the SnO_2-Sb-NRs architecture, providing a direct channel for charge transfer.

3.2 Hydrothermal reaction conditions

3.2.1 Effect of reaction temperature

Figure 5 shows the SEM images of Ti/SnO_2-Sb-NRs synthesized under different temperatures with a fixed reaction time of 24 h. At a low temperature of 150 °C, only some cubic nanoparticles scatter on the surface (Figure 5(a)). As the temperature increases to 180 °C, different sizes of quasi-rod structures can be seen (Figure 5(b)). When the temperature reaches 200 °C and 210 °C, uniform nanorods full develop, and the average widths are 70 nm and 90 nm, respectively (Figure 5(c) and (d)).

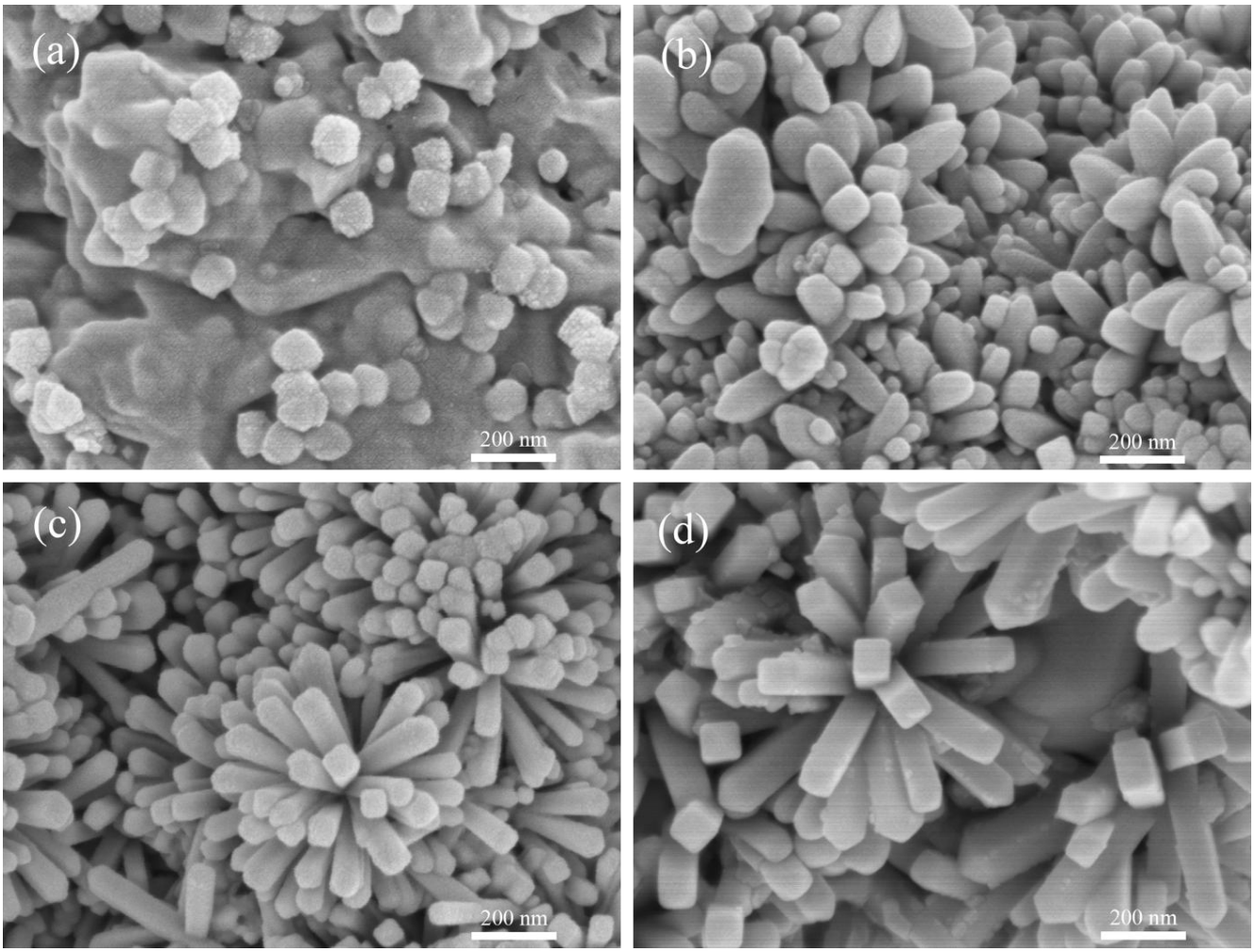

Figure 5. SEM images of electrodes synthesized under different reaction temperatures (a) 150 °C; (b) 180 °C; (c) 200 °C; (d) 210 °C

The effect of the reaction temperature on morphology can be explained by the relationship of the absolute temperature (T) and the relative supersaturation of the solution (S), which can be expressed as,

$$\ln S = \frac{2 \cdot M_{\mathrm{W}} \cdot \gamma}{R \cdot T \cdot \beta \cdot f_{\mathrm{c}}} \tag{1}$$

where M_{w} is the molar mass of $Sn(OH)_4$, γ is the interface energy, β represents the geometric parameters of crystal, and f_c is the particle size of the critical nucleus. As a result, the hydrothermal reaction does not easily occur at a low temperature of 150 °C, and the formation and growth of crystal nucleus is difficult. When the temperature increases to 180 °C, the reaction can be carried out in a large range, and the supersaturation of the solution is greater than the other two groups (200 °C and 210 °C). The crystal nuclei form rapidly, and their quantity increase. However, the growth units diffuse slowly at a relatively low temperature, and it is difficult to supply enough substance for the crystal growth. At a relatively high temperature of 200 °C, the supersaturation of the solution reduces, the formation rate of the crystal nucleus slows, and the diffusion rate of the growth units improves; thus, the crystal achieves its complete growth. When the temperature further improves, a reduction in the amount of nucleation leads to nonuniform nucleation, and the high temperature accelerates the crystal growth rate.

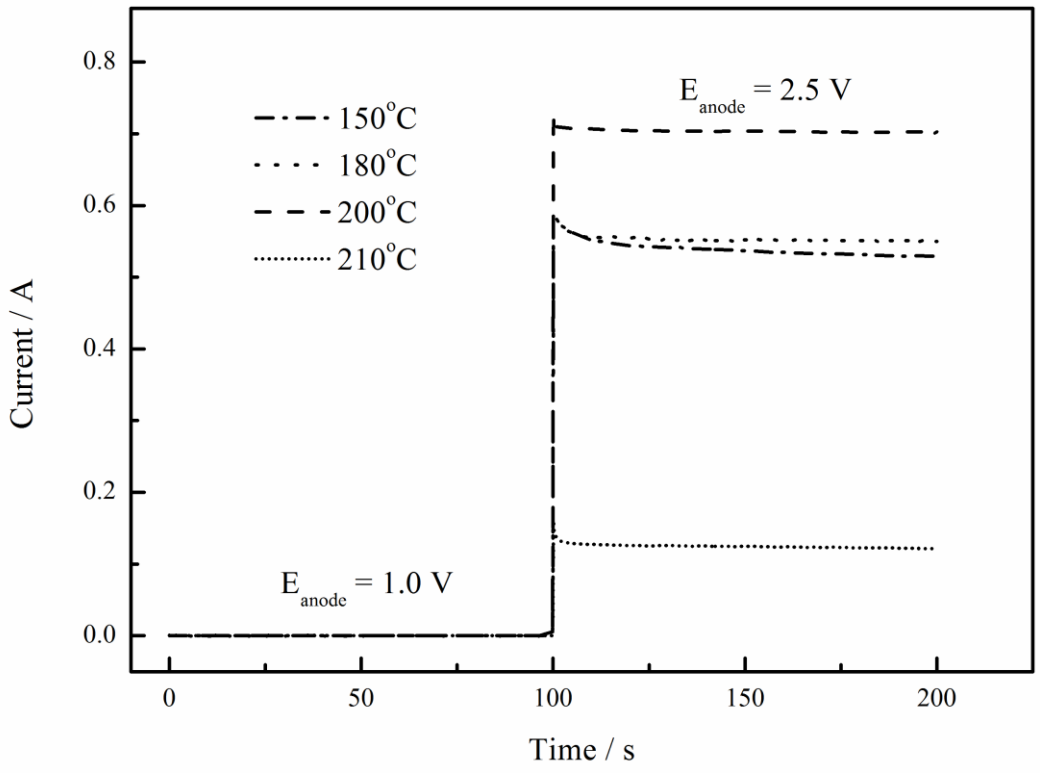

Figure 6. Chronoamperometric responses in a 0.5 M H_2SO_4 solution for electrodes synthesized under different reaction temperatures

The chronoamperometry responses I of the electrodes prepared under different temperatures can be seen in Figure 6, and $I_{\text{r. temp 210°C}} = 0.12$ A < $I_{\text{r. temp 150°C}} = 0.53$ A < $I_{\text{r. temp 180°C}} = 0.55$ A < $I_{\text{r. temp 200°C}} = 0.70$ A. The morphology of the crystals indicates that a crystal growth rate that is too fast leads to the problem of disorder in the crystallinity. In contrast, although the morphology of electrodes synthesized at 150 °C and 180 °C are not nanomaterials, better crystallinities are shown at a low rate of growth. The electrode prepared at 200 °C shows the best behavior in our experiment.

3.2.2 Effect of reaction time

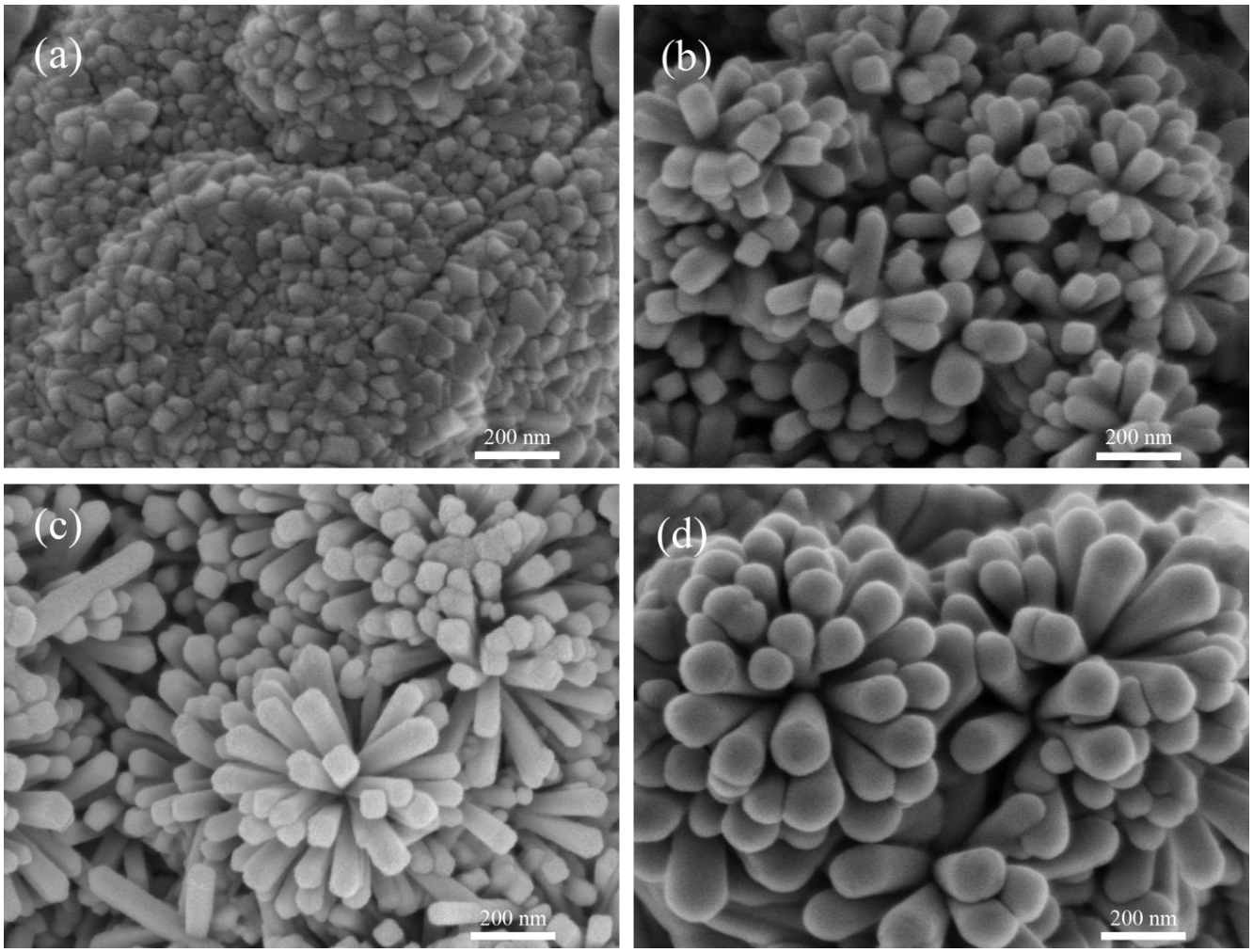

Figure 7. SEM images of electrodes synthesized under different reaction times (a) 12 h; (b) 18 h; (c) 24 h; (d) 30 h

To investigate the effect of reaction time on the formation of SnO_2-Sb nanostructures, SEM images are taken at different growth times at 200 °C, as shown in Figure 7. After the reaction is carried out for 12 h, dense SnO_2-Sb particles with an average width of 50 nm can be identified, and the growth of SnO_2-Sb-NRs is in initial stage (Figure 7(a)). SnO_2-Sb-NRs start to form when the reaction time increases to 18 h; the length and the width are approximately 135 nm and 55 nm (Figure 7(b)). When

the reaction time increases to 24 h, SnO_2-Sb-NRs grow to 235 nm in length and 70 nm in width (Figure 7(c)). In addition, as the time further increases to 30 h, the width of the nanorods increases to approximately 125 nm, which reaches the submicron level (Figure 7(d)). In addition, due to the amplification in diameter, the nanorods come in contact with each other. Similar phenomena have been discussed by Vuong [30], Wang [31] and their co-workers.

Figure 8 shows the chronoamperometry responses of electrodes prepared from different reaction times. The sequence of them is $I_{\text{r. time 12 h}} = 0.19$ A < $I_{\text{r. time 30 h}} = 0.21$ A < $I_{\text{r. time 18 h}} = 0.36$ A < $I_{\text{r. time 24 h}} = 0.70$ A. This implies that the electrochemical performance of the electrodes is closely related to their specific surface area. When the growth time increases to 30 h, the larger size and contact formed between the columns causes the anode to lose the superior characteristics of as nanomaterials.

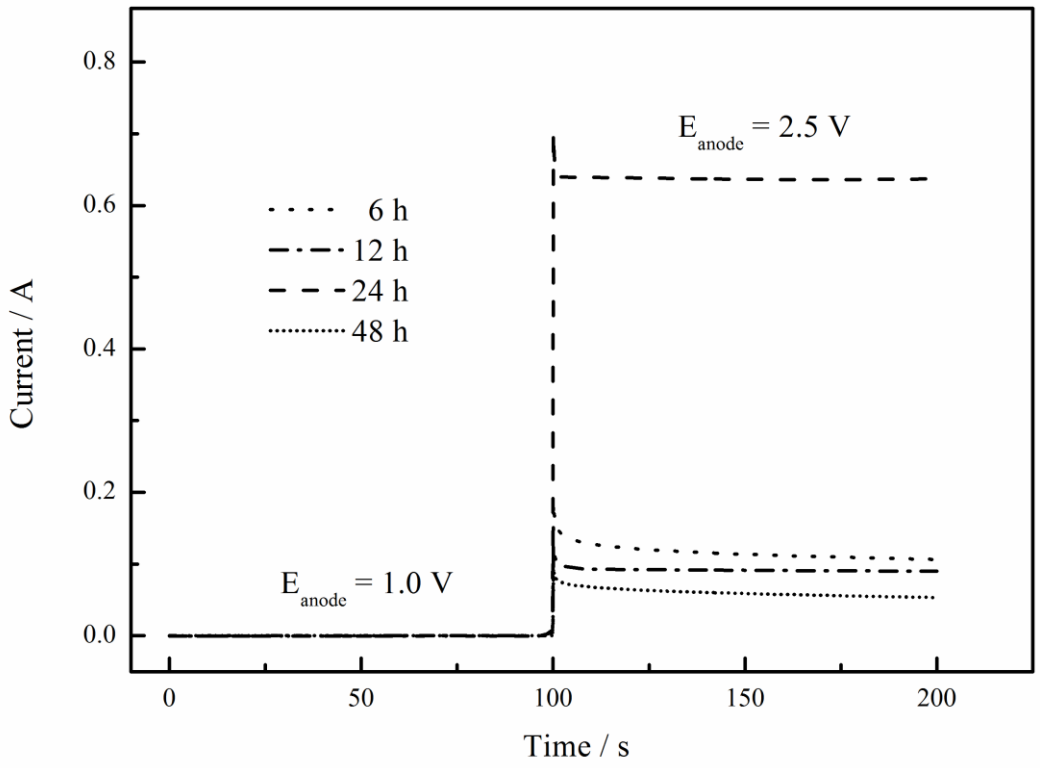

Figure 8. Chronoamperometric responses in a 0.5 M H_2SO_4 solution for electrodes synthesized under different reaction times

3.3 Annealing temperature

An annealing process in this experiment is applied as a high-temperature activation treatment to improve the conductivity and electrocatalytic performance of SnO_2-Sb-NRs [32]. Figure 9 shows the effect of annealing temperature on the electrochemical performance of electrodes, and the result of the

chronoamperometry is $I_{a.\ temp\ 600^{o}C}$ = 0.45 A < $I_{a.\ temp\ 500^{o}C}$ = 0.53 A < $I_{a.\ temp\ 550^{o}C}$ = 0.70 A. During heat treatment in air, the antimony tend to distribute on the surface in the form of Sb^{3+} and distribute internally in the form of Sb^{5+}, and Sb^{5+} can be converted to Sb^{3+} at higher temperatures. Sb^{3+} cations on the surface act as coordination unsaturated sites, which can combine with reactants in the catalytic oxidation reaction. For this reason, when the annealing temperature is 500 °C, the coordination unsaturated sites are less than that of the electrode annealed at 550 °C. However, when the annealing temperature rises to 600 °C, the volatilization of antimony elements is severe, leading to a deterioration in the performance.

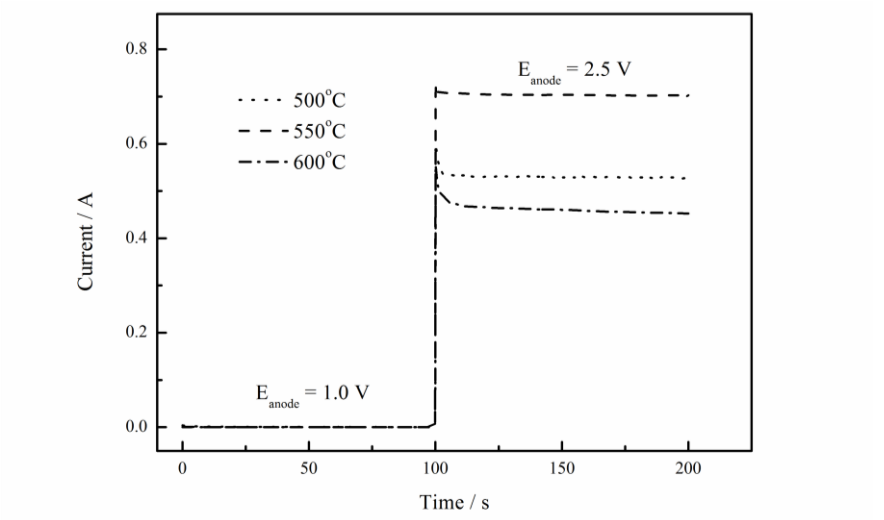

Figure 9. Chronoamperometric responses in a 0.5 M H_2SO_4 solution for electrodes synthesized under different annealing temperatures

3.4 Electrochemical degradation of AR 73

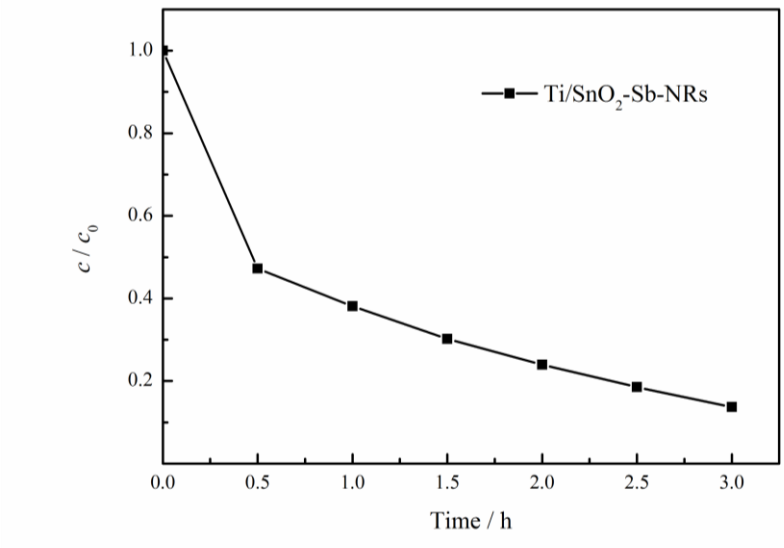

Figure 10. Degradation of AR 73 during the electrochemical oxidation process(c_{AR73} = 1.0 g·L^{-1}, c_{Na2SO4} = 0.1 mol·L^{-1}, i = 50 mA·cm^{-2})

Figure 10 shows the degradation process of AR 73 with time, where c_0 and c are the dye concentrations at the initial and given time, respectively. The Ti/SnO_2-Sb-NRs anode in the experiment is made under the optimal conditions according to the experiments above. The chroma removal rate reaches approximately 86.30% in 3 hours indicating a good electrochemical performance of this anode.

3.5 The growth mechanism of SnO_2-Sb-NRs

SnO_2 is a kind of amphoteric oxide; reaction (2) and (3) can occur in strong alkaline environment, and $Sn(OH)_6^{2-}$ anions are the growth units of SnO_2-NRs. $Sn(OH)_6^{2-}$ decomposes under hydrothermal conditions (reaction (4)), then $Sn(OH)_4$ separates out immediately from the solution, and a continuous dehydration reaction occurs (reaction (5)). Similar to $Sn(OH)_4$, SnO_2 also has a low solubility, smaller size, and higher surface free energy. In this case, SnO_2 crystals tend to agglomerate spontaneously. The sequence of the surface free energy of the rutile structure SnO_2 is (110) < (100) < (101) << (001) [33], and so the difference between the surface free energy values leads to the axial growth direction. Therefore, the growth of nanorods may be introduced along with the face of (110) to form the most stable status.

$$Sn^{4+} + 4OH^- \rightarrow Sn(OH)_4 \quad (2)$$

$$Sn(OH)_4 + 2OH^- \rightarrow Sn(OH)_6^{2-} \quad (3)$$

$$Sn(OH)_6^{2-} \rightleftharpoons Sn(OH)_4 \downarrow + 2OH^- \quad (4)$$

$$Sn(OH)_4 \rightleftharpoons SnO(OH)_2 + H_2O \rightleftharpoons SnO_2 + 2H_2O \quad (5)$$

In this experiment, the SnO_2-Sb layer prepared beforehand by pulsed electrodeposition acts as a growth matrix layer in the hydrothermal reaction, resulting in the occurrence of hetero-nucleation preferentially on the surface of the solids. However, the SnO_2-Sb layer acts as a buffer layer to prevent the exposure of the Ti substrate. With the existence of dangling bonds on the surface of the SnO_2 crystal, the forming SnO_2 in the hydrothermal reaction can combine with the SnO_2 deposited on the substrate. For this reason, the SnO_2-Sb-NRs grow on the matrix through durable chemical bounds.

4. CONCLUSIONS

In this study, SnO_2-Sb nanorods anodes on Ti sheet substrates were prepared under different hydrothermal conditions. SEM images intuitively display the surface morphologies, and the chronoamperometry responses were measured and used to make indirect assessments of the electrochemical performance and stability of the anodes. The possibility of synthesizing SnO_2-Sb-NRs in both strong acid solution and strong alkaline solution was proved. Effects of various solvents, concentrations of precursor solutions, reaction temperatures and times on the morphology and electrochemical performance of the SnO_2-Sb-NRs anodes were indicated. The annealing temperature also had an impact on the stability and conductivity of the anodes. SnO_2-Sb-NRs anode with a relative highest performance was fabricated when the precursor concentration was 0.010 $mol \cdot L^{-1}$, using

ethanol-water (1:1, v/v) as the solvent and a reaction carried out at 200 °C for 24 h, followed by annealing at 550 °C for 2 h.

ACKNOWLEDGEMENT
Our research was supported by the National Natural Science Foundation of China (Grand No. 21276177).

References

1. R.S. Devan, R.A. Patil, J.H. Lin and Y.R. Ma, *Adv. Funct. Mater.*, 22 (2012) 3326.
2. Y.N. Xia, P.D. Yang, Y.G. Sun, Y.Y. Wu, B. Mayers, B. Gates, Y.D. Yin, F. Kim and H.Q. Yan, *Adv. Mater.*, 15 (2003) 353.
3. T.Y. Zhai, X.S. Fang, M.Y. Liao, X.J. Xu, H.B. Zeng, B. Yoshio and D. Golberg, *Sensors-Basel*, 9 (2009) 6504.
4. Z.L. Yang, S.P. Zhao, W. Jiang, X.L. Sun, Y.F. Meng, C.M. Sun and S.J. Ding, *Electrochim. Acta.*, 158 (2015) 321.
5. E. Comini, G. Faglia and G. Sberveglieri, *Appl. Phys. Lett.*, 81 (2002) 1869.
6. A. Kay and M. Gratzel, *Chem. Mater.*, 14 (2002) 2930.
7. J.J. Kong, Z.B. Rui, H.B. Ji and Y.X. Tong, *Catal. Today.*, 258 (2015) 75.
8. Z.W. Pan, Z.R. Dai and Z.L. Wang, *Science*, 291 (2001) 1947.
9. M.L. Lu, T.M. Weng, J.Y. Chen and Y.F. Chen, *Npg. Asia. Mater.*, 4 (2012) 6.
10. H. Choi, H. Jung, D.K. Choi and C.Y. Kim, *J. Nanosci. Nanotechno.*, 16 (2016) 1818.
11. C.Y. Kim, H. Jung, H. Choi and D.K. Choi, *J. Korean. Phys. Soc.*, 68 (2016) 357.
12. D.F. Zhang, L.D. Sun, J.L. Yin and C.H. Yan, *Adv. Mater.*, 15 (2003) 1022.
13. S. Supothina, M. Suwan and A. Wisitsoraat, *J. Ceram. Process. Res.*, 14 (2013) 226.
14. X.L. Xu, Y. Chen, G.H. Zhang, S.Y. Ma, Y. Lu, H.Q. Bian and Q. Chen, *J. Alloy. Compd.*, 703 (2017) 572.
15. N.W. Wang, Y.H. Yang, J. Chen, N.S. Xu and G.W. Yang, *J. Phys. Chem. C.*, 114 (2010) 2909.
16. A. Boumeddiene, F. Bouamra, M.Rérat and H. Belkhir, *Appl. Surf. Sci.*, 284 (2013) 581.
17. X. Liu, G. Zhou, S. Or and Y. Sun, *Rsc. Adv.*, 4 (2014) 51389.
18. B. Yang, J.B. Wang, C.J. Jiang, J.Y. Li, G. Yu, S.B. Deng, S.Y. Lu, P.X. Zhang, C.Z. Zhu and Q.F. Zhuo, *Chem. Eng. J.*, 316 (2017) 296.
19. Y. Liu and M. Liu, *Adv. Funct. Mater.*, 15 (2005) 57.
20. L.A. Ma and T.L. Guo, *Mater. Lett.*, 63 (2009) 295.
21. Q. Kuang, T. Xu, Z.X. Xie, S.C. Lin, R.B. Huang and L.S. Zheng, *J. Mater. Chem.*, 19 (2009) 1019.
22. S.L. Feng, Y.W. Tang and T. Xiao, *J. Phys. Chem. C.*, 113 (2009) 4809.
23. Y.C. Her, J.Y. Wu, Y.R. Lin and S.Y. Tsai, *Appl. Phys. Lett.*, 89 (2006) 582.
24. H.Y. Zhao, F. Li, X.Q. Liu, W.Q. Xiong, B. Chen, H.L. Shao, D.Y. Que, Z. Zhang and Y. Wu, *Electrochim. Acta.*, 166 (2015) 124.
25. L. Xu and Y.F. Lian, *J. Electrochem. Soc.*, 163 (2016) H1144.
26. G. Demazeau, A. Largeteau and Z. Anorg, *Allg. Chem.*, 641 (2015) 159.
27. X.M. Yin, L.B. Chen, C.H. Li, Q.Y. Hao, S. Liu, Q.H. Li, E.D. Zhang and T.H. Wang, *Electrochimi. Acta.*, 56 (2011) 2358.
28. D.F. Zhang, L.D. Sun, J.L. Yin and C.H. Yan, *Adv. Mater.*, 15 (2003) 1022.
29. Y.L. Wang, M. Guo, M. Zhang and X.D. Wang, *Rare. Metals*, 28 (2009) 449.
30. D.D. Vuong, V.X. Hien, K.Q. Trung and N.D. Chien, *Physica. E.*, 44 (2011) 345.
31. Y.L. Wang, M. Guo, M. Zhang and X.D. Wang, *Thin. Solid. Films.*, 518 (2010) 5098.
32. H.J. Jeon, M.K. Jeon, M. Kang and B.H. Choi, *Mater. Lett.*, 59 (2005) 1801.

33. L. Vayssieres and M. Graetzel, *Angew. Chem. Int. Edit.*, 43 (2004) 3666.